

Measurement of ϕ -meson production in Cu+Au collisions at $\sqrt{s_{NN}} = 200$ GeV and U+U collisions at $\sqrt{s_{NN}} = 193$ GeV

N.J. Abdulameer,¹⁵ U. Acharya,²⁰ C. Aidala,^{39,44} N.N. Ajitanand,^{64,*} Y. Akiba,^{59,60,†} R. Akimoto,¹¹ J. Alexander,⁶⁴ M. Alfred,²³ K. Aoki,^{32,59} N. Apadula,^{28,65} H. Asano,^{35,59} E.T. Atomssa,⁶⁵ T.C. Awes,⁵⁵ B. Azmoun,⁷ V. Babintsev,²⁴ M. Bai,⁶ X. Bai,¹⁰ B. Bannier,⁶⁵ K.N. Barish,⁸ S. Bathe,^{5,60} V. Baublis,⁵⁷ C. Baumann,⁷ S. Baumgart,⁵⁹ A. Bazilevsky,⁷ M. Beaumier,⁸ R. Belmont,^{12,53,71} A. Berdnikov,⁶² Y. Berdnikov,⁶² L. Bichon,⁷¹ D. Black,⁸ B. Blankenship,⁷¹ D.S. Blau,^{34,50} J.S. Bok,⁵² V. Borisov,⁶² K. Boyle,⁶⁰ M.L. Brooks,³⁹ J. Bryslawskyj,^{5,8} H. Buesching,⁷ V. Bumazhnov,²⁴ S. Butsyk,⁵¹ S. Campbell,^{13,28} V. Canoa Roman,⁶⁵ C.-H. Chen,⁶⁰ M. Chiu,⁷ C.Y. Chi,¹³ I.J. Choi,²⁵ J.B. Choi,^{30,*} S. Choi,⁶³ P. Christiansen,⁴⁰ T. Chujo,⁷⁰ V. Cianciolo,⁵⁵ B.A. Cole,¹³ M. Connors,²⁰ R. Corliss,⁶⁵ Y. Corrales Morales,³⁹ N. Cronin,^{46,65} N. Crossette,⁴⁶ M. Csanád,¹⁶ T. Csörgő,^{43,73} L. D’Orazio,⁴¹ A. Datta,⁵¹ M.S. Daugherty,¹ G. David,^{7,65} C.T. Dean,³⁹ K. Dehmelt,⁶⁵ A. Denisov,²⁴ A. Deshpande,^{60,65} E.J. Desmond,⁷ L. Ding,²⁸ V. Doomra,⁶⁵ J.H. Do,⁷⁴ O. Drapier,³⁶ A. Drees,⁶⁵ K.A. Drees,⁶ J.M. Durham,³⁹ A. Durum,²⁴ T. Engelmores,¹³ A. Enokizono,^{59,61} R. Esha,⁶⁵ K.O. Eyser,⁷ B. Fadem,⁴⁶ W. Fan,⁶⁵ D.E. Fields,⁵¹ M. Finger, Jr.,⁹ M. Finger,⁹ D. Firak,⁶⁵ D. Fitzgerald,⁴⁴ F. Fleuret,³⁶ S.L. Fokin,³⁴ J.E. Frantz,⁵⁴ A. Franz,⁷ A.D. Frawley,¹⁹ Y. Fukao,³² T. Fusayasu,⁴⁸ K. Gainey,¹ C. Gal,⁶⁵ P. Garg,^{3,65} A. Garishvili,⁶⁷ I. Garishvili,³⁸ M. Giles,⁶⁵ F. Giordano,²⁵ A. Glenn,³⁸ X. Gong,⁶⁴ M. Gonin,³⁶ Y. Goto,^{59,60} R. Granier de Cassagnac,³⁶ N. Grau,² S.V. Greene,⁷¹ M. Grosse Perdekamp,²⁵ T. Gunji,¹¹ H. Guragain,²⁰ Y. Gu,⁶⁴ T. Hachiya,^{49,60} J.S. Haggerty,⁷ K.I. Hahn,¹⁷ H. Hamagaki,¹¹ J. Hanks,⁶⁵ M. Harvey,⁶⁸ S. Hasegawa,²⁹ K. Hashimoto,^{59,61} R. Hayano,¹¹ T.K. Hemmick,⁶⁵ T. Hester,⁸ X. He,²⁰ J.C. Hill,²⁸ A. Hodges,^{20,25} R.S. Hollis,⁸ K. Homma,²² B. Hong,³³ T. Hoshino,²² J. Huang,^{7,39} T. Ichihara,^{59,60} Y. Ikeda,⁵⁹ K. Imai,²⁹ Y. Imazu,⁵⁹ M. Inaba,⁷⁰ A. Iordanova,⁸ D. Isenhower,¹ A. Isinhue,⁴⁶ D. Ivanishchev,⁵⁷ B.V. Jacak,⁶⁵ S.J. Jeon,⁴⁷ M. Jezghani,²⁰ X. Jiang,³⁹ Z. Ji,⁶⁵ B.M. Johnson,^{7,20} K.S. Joo,⁴⁷ D. Jouan,⁵⁶ D.S. Jumper,²⁵ J. Kamin,⁶⁵ S. Kanda,^{11,32} B.H. Kang,²¹ J.H. Kang,⁷⁴ J.S. Kang,²¹ J. Kapustinsky,³⁹ D. Kaway,⁴² A.V. Kazantsev,³⁴ J.A. Key,⁵¹ V. Khachatryan,⁶⁵ P.K. Khandai,³ A. Khanzadeev,⁵⁷ A. Khatiwada,³⁹ K.M. Kijima,²² C. Kim,³³ D.J. Kim,³¹ E.-J. Kim,³⁰ T. Kim,¹⁷ Y.-J. Kim,²⁵ Y.K. Kim,²¹ D. Kincses,¹⁶ A. Kingan,⁶⁵ E. Kistenev,⁷ J. Klatsky,¹⁹ D. Kleinjan,⁸ P. Kline,⁶⁵ T. Koblesky,¹² M. Kofarago,^{16,73} B. Komkov,⁵⁷ J. Koster,⁶⁰ D. Kotchetkov,⁵⁴ D. Kotov,^{57,62} L. Kovacs,¹⁶ F. Krizek,³¹ B. Kurgis,¹⁶ K. Kurita,⁶¹ M. Kurosawa,^{59,60} Y. Kwon,⁷⁴ Y.S. Lai,¹³ J.G. Lajoie,²⁸ D. Larionova,⁶² A. Lebedev,²⁸ D.M. Lee,³⁹ G.H. Lee,³⁰ J. Lee,^{17,66} K.B. Lee,³⁹ K.S. Lee,³³ S.H. Lee,^{28,44,65} M.J. Leitch,³⁹ M. Leitgab,²⁵ B. Lewis,⁶⁵ N.A. Lewis,⁴⁴ S.H. Lim,^{58,74} M.X. Liu,³⁹ X. Li,¹⁰ X. Li,³⁹ D.A. Loomis,⁴⁴ D. Lynch,⁷ S. Lökös,¹⁶ C.F. Maguire,⁷¹ T. Majoros,¹⁵ Y.I. Makdisi,⁶ M. Makek,^{72,75} A. Manion,⁶⁵ V.I. Manko,³⁴ E. Mannel,⁷ M. McCumber,^{12,39} P.L. McGaughey,³⁹ D. McGlinchey,^{12,19,39} C. McKinney,²⁵ A. Meles,⁵² M. Mendoza,⁸ B. Meredith,²⁵ Y. Miake,⁷⁰ T. Mibe,³² A.C. Mignerey,⁴¹ A. Milov,⁷² D.K. Mishra,⁴ J.T. Mitchell,⁷ M. Mitrankova,⁶² Iu. Mitrankov,⁶² S. Miyasaka,^{59,69} S. Mizuno,^{59,70} A. Mohamed,¹⁵ A.K. Mohanty,⁴ S. Mohapatra,⁶⁴ M.M. Mondal,⁶⁵ T. Moon,³³ D.P. Morrison,⁷ M. Moskowicz,⁴⁶ T.V. Moukhanova,³⁴ B. Mulilo,^{33,59,76} T. Murakami,^{35,59} J. Murata,^{59,61} A. Mwai,⁶⁴ T. Nagae,³⁵ S. Nagamiya,^{32,59} J.L. Nagle,¹² M.I. Nagy,¹⁶ I. Nakagawa,^{59,60} Y. Nakamiya,²² K.R. Nakamura,^{35,59} T. Nakamura,⁵⁹ K. Nakano,^{59,69} C. Nattrass,⁶⁷ S. Nelson,¹⁸ P.K. Netrakanti,⁴ M. Nishashi,^{22,59} T. Niida,⁷⁰ R. Nouicer,^{7,60} N. Novitzky,^{31,65,70} T. Novák,^{43,73} G. Nukazuka,^{59,60} A.S. Nyanin,³⁴ E. O’Brien,⁷ C.A. Ogilvie,²⁸ J. Oh,⁵⁸ H. Oide,¹¹ K. Okada,⁶⁰ M. Orosz,¹⁵ J.D. Osborn,⁵⁵ A. Oskarsson,⁴⁰ K. Ozawa,^{32,70} R. Pak,⁷ V. Pantuev,²⁶ V. Papavassiliou,⁵² I.H. Park,^{17,66} S. Park,^{45,63,65} S.K. Park,³³ L. Patel,²⁰ M. Patel,²⁸ S.F. Pate,⁵² J.-C. Peng,²⁵ W. Peng,⁷¹ D.V. Perepelitsa,^{12,13} G.D.N. Perera,⁵² D.Yu. Peressounko,³⁴ C.E. PerezLara,⁶⁵ J. Perry,²⁸ R. Petti,^{7,65} C. Pinkenburg,⁷ R.P. Pisani,⁷ M. Potekhin,⁷ A. Pun,⁵⁴ M.L. Purschke,⁷ H. Qu,¹ P.V. Radzevich,⁶² J. Rak,³¹ N. Ramasubramanian,⁶⁵ I. Ravinovich,⁷² K.F. Read,^{55,67} D. Reynolds,⁶⁴ V. Riabov,^{50,57} Y. Riabov,^{57,62} E. Richardson,⁴¹ D. Richford,⁵ N. Rivelis,⁵⁴ D. Roach,⁷¹ S.D. Rolnick,⁸ M. Rosati,²⁸ J. Runchey,²⁸ M.S. Ryu,²¹ B. Sahlmueeller,⁶⁵ N. Saito,³² T. Sakaguchi,⁷ H. Sako,²⁹ V. Samsonov,^{50,57} M. Sarsour,²⁰ S. Sato,²⁹ S. Sawada,³² K. Sedgwick,⁸ J. Seele,⁶⁰ R. Seidl,^{59,60} Y. Sekiguchi,¹¹ A. Sen,^{20,28} R. Seto,⁸ P. Sett,⁴ D. Sharma,⁶⁵ A. Shaver,²⁸ I. Shein,²⁴ Z. Shi,³⁹ M. Shibata,⁴⁹ T.-A. Shibata,^{59,69} K. Shigaki,²² M. Shimomura,^{28,49} K. Shoji,⁵⁹ P. Shukla,⁴ A. Sickles,^{7,25} C.L. Silva,³⁹ D. Silvermyr,^{40,55} B.K. Singh,³ C.P. Singh,³ V. Singh,³ M. Skolnik,⁴⁶ M. Slunečka,⁹ K.L. Smith,¹⁹ S. Solano,⁴⁶ R.A. Soltz,³⁸ W.E. Sondheim,³⁹ S.P. Sorensen,⁶⁷ I.V. Sourikova,⁷ P.W. Stankus,⁵⁵ P. Steinberg,⁷ E. Stenlund,⁴⁰ M. Stepanov,^{42,*} A. Ster,⁷³ S.P. Stoll,¹² M.R. Stone,¹² T. Sugitate,²² A. Sukhanov,⁷ J. Sun,⁶⁵ Z. Sun,¹⁵ R. Takahama,⁴⁹ A. Takahara,¹¹ A. Taketani,^{59,60} Y. Tanaka,⁴⁸ K. Tanida,^{29,60,63} M.J. Tannenbaum,⁷ S. Tarafdar,^{3,71} A. Taranenko,^{50,64} E. Tennant,⁵² A. Timilsina,²⁸ T. Todoroki,^{59,60,70} M. Tomášek,^{14,27} H. Torii,¹¹

R.S. Towell,¹ I. Tserruya,⁷² Y. Ueda,²² B. Ujvari,¹⁵ H.W. van Hecke,³⁹ M. Vargyas,^{16,73} E. Vazquez-Zambrano,¹³ A. Veicht,¹³ J. Velkovska,⁷¹ M. Virius,¹⁴ V. Vrba,^{14,27} E. Vznuzdaev,⁵⁷ R. Vértesi,⁷³ X.R. Wang,^{52,60} Z. Wang,⁵ D. Watanabe,²² K. Watanabe,^{59,61} Y. Watanabe,^{59,60} Y.S. Watanabe,^{11,32} F. Wei,⁵² S. Whitaker,²⁸ S. Wolin,²⁵ C.P. Wong,^{20,39} C.L. Woody,⁷ M. Wysocki,⁵⁵ B. Xia,⁵⁴ Y.L. Yamaguchi,^{11,65} A. Yanovich,²⁴ S. Yokkaichi,^{59,60} I. Yoon,⁶³ I. Younus,^{37,51} Z. You,³⁹ I.E. Yushmanov,³⁴ W.A. Zajc,¹³ A. Zelenski,⁶ S. Zhou,¹⁰ and L. Zou⁸

(PHENIX Collaboration)

¹Abilene Christian University, Abilene, Texas 79699, USA

²Department of Physics, Augustana University, Sioux Falls, South Dakota 57197, USA

³Department of Physics, Banaras Hindu University, Varanasi 221005, India

⁴Bhabha Atomic Research Centre, Bombay 400 085, India

⁵Baruch College, City University of New York, New York, New York, 10010 USA

⁶Collider-Accelerator Department, Brookhaven National Laboratory, Upton, New York 11973-5000, USA

⁷Physics Department, Brookhaven National Laboratory, Upton, New York 11973-5000, USA

⁸University of California-Riverside, Riverside, California 92521, USA

⁹Charles University, Ovocný trh 5, Praha 1, 116 36, Prague, Czech Republic

¹⁰Science and Technology on Nuclear Data Laboratory, China Institute of Atomic Energy, Beijing 102413, People's Republic of China

¹¹Center for Nuclear Study, Graduate School of Science, University of Tokyo, 7-3-1 Hongo, Bunkyo, Tokyo 113-0033, Japan

¹²University of Colorado, Boulder, Colorado 80309, USA

¹³Columbia University, New York, New York 10027 and Nevis Laboratories, Irvington, New York 10533, USA

¹⁴Czech Technical University, Zikova 4, 166 36 Prague 6, Czech Republic

¹⁵Debrecen University, H-4010 Debrecen, Egyetem tér 1, Hungary

¹⁶ELTE, Eötvös Loránd University, H-1117 Budapest, Pázmány P. s. 1/A, Hungary

¹⁷Ewha Womans University, Seoul 120-750, Korea

¹⁸Florida A&M University, Tallahassee, FL 32307, USA

¹⁹Florida State University, Tallahassee, Florida 32306, USA

²⁰Georgia State University, Atlanta, Georgia 30303, USA

²¹Hanyang University, Seoul 133-792, Korea

²²Hiroshima University, Kagamiyama, Higashi-Hiroshima 739-8526, Japan

²³Department of Physics and Astronomy, Howard University, Washington, DC 20059, USA

²⁴IHEP Protvino, State Research Center of Russian Federation, Institute for High Energy Physics, Protvino, 142281, Russia

²⁵University of Illinois at Urbana-Champaign, Urbana, Illinois 61801, USA

²⁶Institute for Nuclear Research of the Russian Academy of Sciences, prospekt 60-letiya Oktyabrya 7a, Moscow 117312, Russia

²⁷Institute of Physics, Academy of Sciences of the Czech Republic, Na Slovance 2, 182 21 Prague 8, Czech Republic

²⁸Iowa State University, Ames, Iowa 50011, USA

²⁹Advanced Science Research Center, Japan Atomic Energy Agency, 2-4

Shirakata Shirane, Tokai-mura, Naka-gun, Ibaraki-ken 319-1195, Japan

³⁰Jeonbuk National University, Jeonju, 54896, Korea

³¹Helsinki Institute of Physics and University of Jyväskylä, P.O.Box 35, FI-40014 Jyväskylä, Finland

³²KEK, High Energy Accelerator Research Organization, Tsukuba, Ibaraki 305-0801, Japan

³³Korea University, Seoul 02841, Korea

³⁴National Research Center "Kurchatov Institute", Moscow, 123098 Russia

³⁵Kyoto University, Kyoto 606-8502, Japan

³⁶Laboratoire Leprince-Ringuet, Ecole Polytechnique, CNRS-IN2P3, Route de Saclay, F-91128, Palaiseau, France

³⁷Physics Department, Lahore University of Management Sciences, Lahore 54792, Pakistan

³⁸Lawrence Livermore National Laboratory, Livermore, California 94550, USA

³⁹Los Alamos National Laboratory, Los Alamos, New Mexico 87545, USA

⁴⁰Department of Physics, Lund University, Box 118, SE-221 00 Lund, Sweden

⁴¹University of Maryland, College Park, Maryland 20742, USA

⁴²Department of Physics, University of Massachusetts, Amherst, Massachusetts 01003-9337, USA

⁴³MATE, Laboratory of Femtoscopy, Károly Róbert Campus, Gyöngyös, Hungary

⁴⁴Department of Physics, University of Michigan, Ann Arbor, Michigan 48109-1040, USA

⁴⁵Mississippi State University, Mississippi State, Mississippi 39762, USA

⁴⁶Muhlenberg College, Allentown, Pennsylvania 18104-5586, USA

⁴⁷Myongji University, Yongin, Kyonggido 449-728, Korea

⁴⁸Nagasaki Institute of Applied Science, Nagasaki-shi, Nagasaki 851-0193, Japan

⁴⁹Nara Women's University, Kita-uoya Nishi-machi Nara 630-8506, Japan

⁵⁰National Research Nuclear University, MEPhI, Moscow Engineering Physics Institute, Moscow, 115409, Russia

⁵¹University of New Mexico, Albuquerque, New Mexico 87131, USA

⁵²New Mexico State University, Las Cruces, New Mexico 88003, USA

⁵³Physics and Astronomy Department, University of North Carolina at Greensboro, Greensboro, North Carolina 27412, USA

⁵⁴Department of Physics and Astronomy, Ohio University, Athens, Ohio 45701, USA

- ⁵⁵ Oak Ridge National Laboratory, Oak Ridge, Tennessee 37831, USA
- ⁵⁶ IPN-Orsay, Univ. Paris-Sud, CNRS/IN2P3, Université Paris-Saclay, BP1, F-91406, Orsay, France
- ⁵⁷ PNPI, Petersburg Nuclear Physics Institute, Gatchina, Leningrad region, 188300, Russia
- ⁵⁸ Pusan National University, Pusan 46241, Korea
- ⁵⁹ RIKEN Nishina Center for Accelerator-Based Science, Wako, Saitama 351-0198, Japan
- ⁶⁰ RIKEN BNL Research Center, Brookhaven National Laboratory, Upton, New York 11973-5000, USA
- ⁶¹ Physics Department, Rikkyo University, 3-34-1 Nishi-Ikebukuro, Toshima, Tokyo 171-8501, Japan
- ⁶² Saint Petersburg State Polytechnic University, St. Petersburg, 195251 Russia
- ⁶³ Department of Physics and Astronomy, Seoul National University, Seoul 151-742, Korea
- ⁶⁴ Chemistry Department, Stony Brook University, SUNY, Stony Brook, New York 11794-3400, USA
- ⁶⁵ Department of Physics and Astronomy, Stony Brook University, SUNY, Stony Brook, New York 11794-3800, USA
- ⁶⁶ Sungkyunkwan University, Suwon, 440-746, Korea
- ⁶⁷ University of Tennessee, Knoxville, Tennessee 37996, USA
- ⁶⁸ Texas Southern University, Houston, TX 77004, USA
- ⁶⁹ Department of Physics, Tokyo Institute of Technology, Oh-okayama, Meguro, Tokyo 152-8551, Japan
- ⁷⁰ Tomonaga Center for the History of the Universe, University of Tsukuba, Tsukuba, Ibaraki 305, Japan
- ⁷¹ Vanderbilt University, Nashville, Tennessee 37235, USA
- ⁷² Weizmann Institute, Rehovot 76100, Israel
- ⁷³ Institute for Particle and Nuclear Physics, Wigner Research Centre for Physics, Hungarian Academy of Sciences (Wigner RCP, RMKI) H-1525 Budapest 114, POBox 49, Budapest, Hungary
- ⁷⁴ Yonsei University, IPAP, Seoul 120-749, Korea
- ⁷⁵ Department of Physics, Faculty of Science, University of Zagreb, Bijenička c. 32 HR-10002 Zagreb, Croatia
- ⁷⁶ Department of Physics, School of Natural Sciences, University of Zambia, Great East Road Campus, Box 32379, Lusaka, Zambia
- (Dated: July 25, 2022)

The PHENIX experiment reports systematic measurements at the Relativistic Heavy Ion Collider of ϕ -meson production in asymmetric Cu+Au collisions at $\sqrt{s_{NN}} = 200$ GeV and in U+U collisions at $\sqrt{s_{NN}} = 193$ GeV. Measurements were performed via the $\phi \rightarrow K^+ K^-$ decay channel at midrapidity $|\eta| < 0.35$. Features of ϕ -meson production measured in Cu+Cu, Cu+Au, Au+Au, and U+U collisions were found to not depend on the collision geometry, which was expected because the yields are averaged over the azimuthal angle and follow the expected scaling with nuclear-overlap size. The elliptic flow of the ϕ meson in Cu+Au, Au+Au, and U+U collisions scales with second order participant eccentricity and the length scale of the nuclear overlap region (estimated with the number of participating nucleons). At moderate p_T , ϕ -meson production measured in Cu+Au and U+U collisions is consistent with coalescence-model predictions, whereas at high p_T the production is in agreement with expectations for in-medium energy loss of parent partons prior to their fragmentation. The elliptic flow for ϕ mesons measured in Cu+Au and U+U collisions is well described by a (2+1)D viscous-hydrodynamic model with specific-shear viscosity $\eta/s = 1/4\pi$.

I. INTRODUCTION

The formation of the quark-gluon plasma (QGP) has been established by experiments at the Relativistic Heavy Ion Collider (RHIC) [1–5] and later at the Large Hadron Collider (LHC) [6–9]. Since then, one of the main goals of high-energy nuclear physics, including the PHENIX experiment [10], is to quantify and characterize the properties of the QGP. Measurements of light-hadron production in collision systems with different geometries are commonly used for the systematic experimental study of the evolution of the medium created in high-energy nuclear collisions, including the QGP phase.

The processes of QGP formation and evolution depend on the initial conditions. The initial conditions include the collision-system energy, the nuclear-overlap

size and shape, and nuclear modification of the parton-distribution functions [11]. In the most central Cu+Au collisions, the Cu ion is fully occluded by the Au ion, which might lead to significantly larger suppression of particle yields than for symmetric systems like Cu+Cu and Au+Au [12]. Collisions of uranium nuclei, which are highly deformed, provide different collision configurations depending on their orientation relative to the reaction plane. On average, comparing to symmetric systems, the nuclear-overlap region in Cu+Au and U+U collisions has additional asymmetry along the impact-parameter orientation. In addition to different nuclear thicknesses, this leads to initial conditions that are different from those of symmetric systems. Thus, comparison of particle production measured in Cu+Au and U+U collision and symmetric systems is a useful tool to study the influence of initial conditions on the evolution of heavy ion collisions.

Measurements of light-hadron transverse-momentum (p_T) spectra provide probes of QGP effects, such as jet quenching [13] and strangeness enhancement [14].

* Deceased

† PHENIX Spokesperson: akiba@rcf.rhic.bnl.gov

Jet quenching manifests as a suppression of high- p_T hadron yields, due to parton energy losses in the hot and dense medium. Strangeness enhancement can be observed as the increase of strange and hidden-strange hadron yields in nucleus-nucleus collisions relative to $p+p$ collision scaled by the appropriate number of binary nucleon-nucleon collisions. Hadronization via the parton-coalescence (recombination) mechanism [15–17] should be considered to quantify strangeness-enhancement effect. Because the degree of strangeness saturation and parton energy loss are sensitive to initial conditions [13, 14], measurements of strange and hidden-strange hadron production can shed light on the physics of the initial conditions.

The investigation of elliptic-flow coefficients (v_2) can provide insight on how the initial transverse coordinate-space anisotropy of heavy ion collisions is converted to a momentum-space anisotropy in the transverse plane [18]. Previous studies of v_2 at RHIC in symmetric collision systems (Au+Au, Cu+Cu) show that v_2 values for light hadrons depend on the number of valence quarks in the hadron (n_q), the second order participant eccentricity (ε_2) and the number of nucleons participating in the interaction ($\langle N_{\text{part}} \rangle$) [19, 20]. The comparison of obtained results to the hydrodynamic model predictions suggests that the QGP has properties of a nearly perfect fluid [21]. Therefore, hadronic elliptic flow is sensitive to the shape and the size of the nuclear-overlap region. Measurements of v_2 for light hadrons in Cu+Au and U+U collisions can reveal underlying physics mechanisms of its development.

The ϕ meson is considered to be a clean probe of QGP properties. It has an Okubo-Zweig-Iizuka (OZI) suppressed-interaction cross section with non-strange hadrons and a lifetime (42 fm/c [22]) significantly longer than that of the QGP (~ 10 fm/c [2]). Therefore, ϕ mesons mostly decay outside the fireball, and along with their daughter particles rescatter less frequently in the hadronization phase. Consequently, the kinematic properties are primarily controlled by conditions in the early partonic phase and less affected in the hadronization stage. The ϕ vector meson is the nearly pure lightest bound state of $s\bar{s}$ quarks. Accordingly, measurements of the ϕ -meson p_T spectra in various collision systems can contribute to the understanding of strangeness enhancement, along with energy loss and coalescence. The comparison of v_2 values for ϕ mesons to nonOZI suppressed π^\pm mesons and (anti)protons can indicate a role of hadronization stage in v_2 development.

The PHENIX experiment has measured ϕ -meson production in asymmetric Cu+Au collisions at $\sqrt{s_{NN}} = 200$ GeV and in the largest collision system at RHIC U+U at $\sqrt{s_{NN}} = 193$ GeV. The influence of initial conditions on ϕ -meson production is investigated by measuring invariant p_T spectra, R_{AB} , and v_2 in Cu+Au and U+U collisions. The obtained results are compared to theoretical calculations based on viscous hydrodynamics (iEBE-VISHNU [23]), a-multiphase-transport model (AMPT [24]) and a leading-order (LO)

perturbative quantum chromodynamics (pQCD) model (PYTHIA/Angantyr [25]).

II. DATA ANALYSIS

A. Data sets and event selection

The ϕ -meson production analyses are based on data sets collected from Cu+Au collisions at $\sqrt{s_{NN}} = 200$ GeV and U+U collisions at $\sqrt{s_{NN}} = 193$ GeV by the PHENIX detector during the 2012 running period. Figure 1 shows the relevant experimental setup [10].

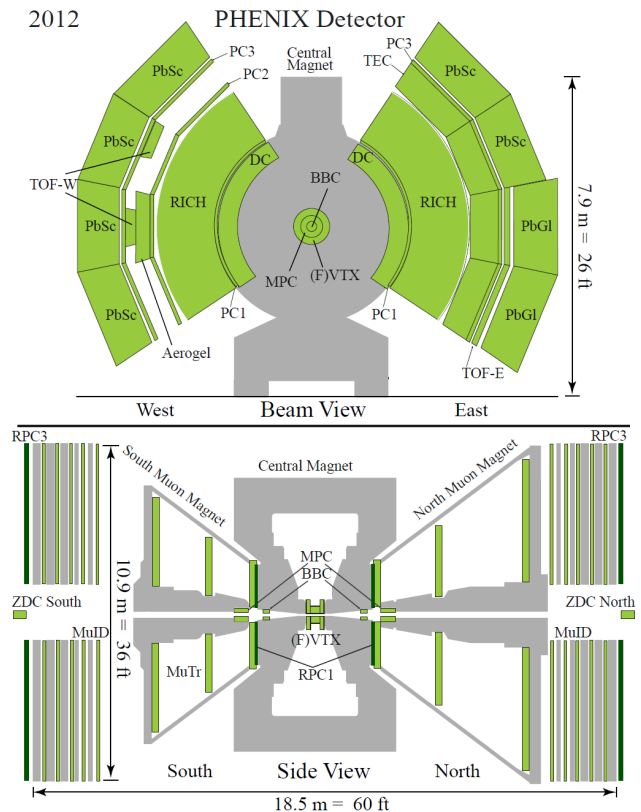


FIG. 1. The PHENIX detector configuration for data taking in 2012.

The PHENIX detector has two beam-beam counters (BBC) [26] located at ± 144 cm from the nominal interaction point, each of which covers $0 < \phi < 2\pi$ in azimuthal angle and $3.1 < |\eta| < 3.9$ in pseudorapidity. The minimum-bias (MB) trigger requires at least two phototubes on each side of the BBC to have a signal above the noise threshold. The MB definition is satisfied by $93 \pm 2\%$ of the inelastic Cu+Au and U+U cross section. The online z -vertex of the event is determined by the time difference between signals from the north and south arms of the BBC, and is required to be within ± 30 cm from the center of the detector. The recorded luminosity of Cu+Au and U+U collisions is 27.0 nb^{-1} and 736

μb^{-1} , respectively.

B. Centrality and event plane azimuthal angle

The event centrality class in Cu+Au and U+U collisions is determined as a percentile of the absolute values of the total charge measured in the north and south BBCs [27]. Glauber model Monte-Carlo simulations [28] that include the responses of the BBC are used to estimate the average values of the number of participating nucleons $\langle N_{\text{part}} \rangle$, the number of binary nucleon-nucleon collisions $\langle N_{\text{coll}} \rangle$, and the second-harmonic eccentricity ε_2 for each centrality class. Two parameterizations of the deformed Woods-Saxon distribution for Uranium nuclei are considered because there is no single universally accepted parameterization of the U nucleus. Two Monte-Carlo simulations were produced to provide two sets, Glauber 1 [29] and Glauber 2 [30], of the collision geometry parameters. The $\langle N_{\text{part}} \rangle$, $\langle N_{\text{coll}} \rangle$, and ε_2 values for Cu+Au and U+U collisions are presented in Tables I-II.

TABLE I. Values of $\langle N_{\text{coll}} \rangle$ and $\langle N_{\text{part}} \rangle$ for MB and centrality ranges in Cu+Au collisions at $\sqrt{s_{NN}} = 200$ GeV and U+U collisions at $\sqrt{s_{NN}} = 193$ GeV

Coll.	Glauber	Centrality	$\langle N_{\text{coll}} \rangle$	$\langle N_{\text{part}} \rangle$
Cu+Au	Glauber Ref. [28]	MB	108 ± 11	61.1 ± 2.7
		0%–20%	313 ± 28	154 ± 4
		20%–40%	129 ± 12	80.4 ± 3.3
		40%–60%	41.8 ± 5.3	34.9 ± 2.8
		20%–60%	85.6 ± 8.9	57.7 ± 3.1
		60%–80%	10.1 ± 2.0	12.1 ± 1.9
U+U	Glauber 1 Ref. [29]	0%–80%	342 ± 30	143 ± 5
		0%–20%	935 ± 98	330 ± 6
		20%–40%	335 ± 33	159 ± 7
		40%–60%	81.0 ± 13.1	64.8 ± 5.9
		60%–80%	17.5 ± 3.9	17.8 ± 3.2
		60%–80%	10.1 ± 2.0	12.1 ± 1.9
U+U	Glauber 2 Ref. [30]	0%–80%	375 ± 42	144 ± 5
		0%–20%	999 ± 114	330 ± 6
		20%–40%	375 ± 46	161 ± 7
		40%–60%	110 ± 15	65.8 ± 5.8
		60%–80%	19.8 ± 4.4	18.2 ± 3.2
		60%–80%	10.1 ± 2.0	12.1 ± 1.9

TABLE II. Values of ε_2 for Cu+Au collisions at $\sqrt{s_{NN}} = 200$ GeV and U+U collisions at $\sqrt{s_{NN}} = 193$ GeV.

Collisions	Glauber	Centrality	ε_2
Cu+Au	Glauber [28]	0%–20%	0.171 ± 0.009
		20%–40%	0.318 ± 0.009
		40%–60%	0.480 ± 0.016
		20%–60%	0.399 ± 0.012
U+U	Glauber 1 [29]	0%–50%	0.310 ± 0.024
U+U	Glauber 2 [30]	0%–50%	0.366 ± 0.013

The azimuthal angle of the event plane Ψ_2 is determined using the forward silicon-vertex detector

(FVTX) [31] in Cu+Au collisions and the muon-piston calorimeter (MPC) [32] in U+U collisions. The Ψ_2 obtained with the BBC detector is used to estimate systematic uncertainties in both collision systems. The FVTX is a silicon detector designed to provide precise tracking for charged particles entering the muon spectrometer before undergoing multiple scattering in the hadron absorber. The FVTX comprises two arms, north and south, covering a large rapidity pseudorapidity $1 < |\eta| < 3$. The MPC is a lead-tungstate calorimeter equipped with PbWO₄ crystal scintillator towers. The north arm of the MPC has 220 towers spanning pseudorapidities $3.1 < \eta < 3.9$, while the south MPC has 196 towers spanning $-3.7 < \eta < -3.1$. The MPC covers almost the same η range as the BBC, but has finer granularity and detects both charged and neutral particles, and hence provides better event-plane resolution. The event-plane angle is determined by the event flow vector Q_2 [33]. The Q -vectors are recentered according to the procedure described in [33]. The raw event-plane angle is estimated by:

$$n\Psi_n^{\text{Raw}} = \arctan \frac{Q_{n,x}}{Q_{n,y}}, \quad (1)$$

where $Q_{n,x}$ and $Q_{n,y}$ are the x and y projections of the flow vector. The flattening procedure described in [33, 34] is applied to the Ψ_2^{Raw} distributions to remove detector acceptance effects. The resolution $\text{Res}(\Psi_2)$ values are evaluated using the three-subevent method [34] correlating independent measurements made in the FVTX or MPC, BBC and the central arms (CNT) and are presented in Table III.

TABLE III. Values of the second-order event-plane resolution $\text{Res}(\Psi_2)$ in Cu+Au collisions at $\sqrt{s_{NN}} = 200$ GeV and U+U collisions at $\sqrt{s_{NN}} = 193$ GeV.

Collisions	Centrality	$\text{Res}(\Psi_2)$
Cu+Au	0%–20%	0.374
	20%–40%	0.404
	40%–60%	0.304
	20%–60%	0.357
U+U	0%–50%	0.495

C. The ϕ -meson raw yield extraction

The yields of ϕ mesons (N_ϕ) are extracted by invariant-mass analysis via decay into oppositely charged kaons ($\phi \rightarrow K^+ K^-$). For $\phi \rightarrow K^+ K^-$ decay, the Particle Data Group [35] values are

- mass = 1019.455 ± 0.020 MeV/ c^2 ,
- width = 4.26 ± 0.04 MeV, and
- branching ratio = 48.9 ± 0.5 %.

The analysis method follows a consolidated technique described extensively in Refs. [36–40].

The measurements use two PHENIX central arms, each covering $|\eta| < 0.35$ in pseudorapidity and 90° in azimuthal angle. The central arms include a tracking system [41], which comprises drift chambers and pad chambers. The tracking system is used for three-momentum-components determination for every track with a typical resolution of $\delta p/p = 0.7\% \oplus 1.1\% \times p$ [GeV/c]. The time of flight (τ_f) for hadrons is measured using the east-arm time-of-flight detector (TOFE) [42, 43] and the BBC. Information from the tracking system and τ_f allows for clear π/K separation for $0.3 < p_T < 2.2$ GeV/c [44].

In each event, all tracks of opposite charge that pass the selection criteria [36, 37] are paired to form the invariant-mass distribution (m_{KK}) in the selected ϕ -meson p_T and event-centrality ranges. To maximize the statistical significance and the p_T reach of the measurements, three different pair-combination techniques are used. The first (“no PID”) does not require identification of charged tracks in the final state and assumes that all tracks are kaons. The second (“one-kaon PID”) requires identification of only one kaon in the TOFE subsystem. The third technique (“two-kaons PID”) identifies both kaons in the TOFE. Each technique has advantages and disadvantages described in Ref. [37]. Both approaches with kaon identification have a more favorable signal-to-background ratio compared to the “no PID” technique, but due to the small acceptance of the TOFE detector and its limited capability to identify kaons at $p_T > 2.2$ GeV/c, these techniques have a limited p_T reach. The “no PID” approach allows the measurements to be extended towards higher p_T as it has substantially larger acceptance and a phase-space volume available for daughter kaons. All mentioned analysis techniques have a significant overlap in p_T and different sources of systematic uncertainties providing a valuable consistency check. The results obtained with different methods can not be directly averaged [37]. Therefore, to obtain the smallest statistical uncertainties for measurements of ϕ -meson p_T spectra and v_2 values, the “no PID” approach is used at $p_T > 2.2$ and 2.0 GeV/c respectively, the “one-kaon PID” is used at lower p_T values, and the “two-kaon PID” is used for cross check and to estimate systematic uncertainties. Figure 2 shows a typical invariant-mass distribution obtained using each of the three PID methods.

A large background that comes from random combinations of uncorrelated hadrons affects the invariant-mass spectrum. To estimate this background, a mixed-event technique [45] is applied that uses unlike-sign kaon tracks taken from different events with similar characteristics (i.e. centrality and z -vertex). After subtraction, distributions are fitted with the sum of a Breit-Wigner mass-distribution function and a polynomial of the third order, which describe the ϕ -meson signal and the residual background, respectively. The ϕ -meson raw yields are obtained as the integral of the mass distribution in a window of ± 9 MeV/c² around the ϕ meson mass after

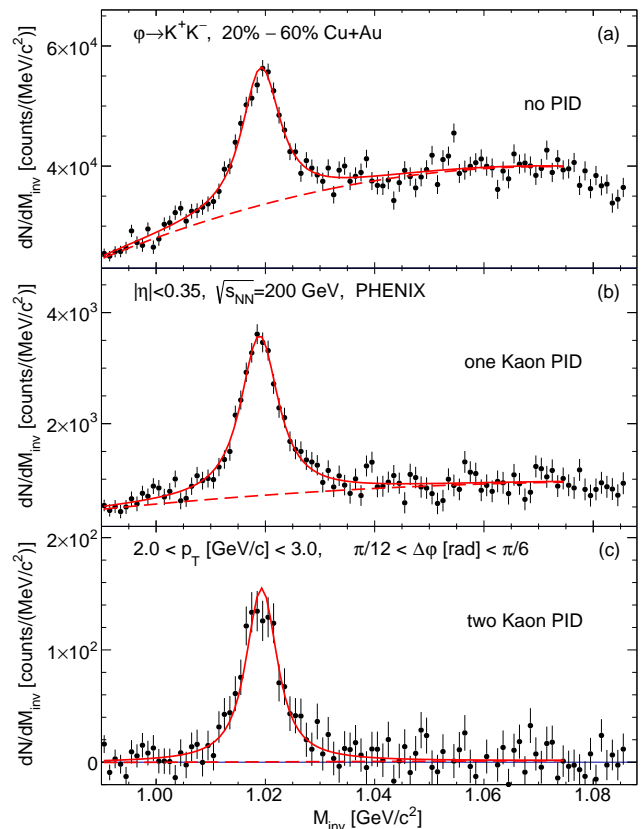


FIG. 2. Examples of invariant-mass distributions for the K^+K^- pairs in 20%-60% Cu+Au collisions at $\sqrt{s_{NN}} = 200$ GeV, obtained with the (a) no PID, (b) one-kaon PID, and (c) two-kaons PID methods after subtraction of the uncorrelated background estimated using the event-mixing technique. Plots correspond to integrated p_T for $2.0 < p_T < 3.0$ GeV/c and $\pi/12 < \Delta\phi[\text{rad}] < \pi/6$. Spectra are fitted to the sum of a Voigt function and polynomial of the third order, which described the ϕ -meson signal and the residual background, respectively.

subtracting the residual background.

D. Invariant spectra and nuclear modification factors

The p_T -differential yields are corrected for the ϕ -meson reconstruction efficiency and acceptance of the detector, as described in [36, 37], using GEANT3 [46] Monte-Carlo simulations for the 2012 configuration of the PHENIX detector. The selection criteria for kaons and ϕ -meson candidates are the same in Monte Carlo and real data. The acceptance and reconstruction efficiency $\varepsilon_{\text{eff}}(p_T)$ are evaluated as a ratio of reconstructed to generated ϕ mesons for the appropriate kinematic bin and event centrality in simulation.

Invariant transverse-momentum spectra of ϕ mesons

are calculated as:

$$\frac{1}{2\pi p_T} \frac{d^2 N}{dp_T dy} = \frac{1}{2\pi p_T} \frac{1}{N_{\text{event}} Br} \frac{1}{\varepsilon_{\text{eff}}(p_T)} \frac{N_\phi(\Delta p_T)}{\Delta p_T \Delta y} \quad (2)$$

where p_T is the transverse momentum, Δp_T is the transverse momentum interval, Δy is the rapidity interval, and N_{event} is the number of events in the selected centrality bin. Nuclear-modification factors (R_{AB}) are used to study modifications to particle spectra [47] and are calculated as

$$R_{AB} = \frac{\sigma_{pp}^{\text{inel}}}{\langle N_{\text{coll}} \rangle} \cdot \frac{d^2 N_{AB}/dy dp_T}{d^2 \sigma_{pp}/dy dp_T}, \quad (3)$$

where $d^2 N_{AB}/dy dp_T$ is the per-event yield of particle production in $A+B$ collisions, $d^2 \sigma_{pp}/dy dp_T$ is the production cross section in $p+p$ collisions, and $\sigma_{pp}^{\text{inel}} = 42.2$ mb [48] is the total inelastic cross section in $p+p$ collisions.

E. Elliptic Flow

A robust method [38–40] is used to study the elliptic flow of resonance particles, such as the ϕ meson. To obtain the azimuthal-angle dependence of ϕ -meson production, the ϕ -meson raw yields are measured in a selected p_T range as a function of the K^+K^- pair angle with respect to the reaction-plane orientation in six equally spaced bins of $\Delta\varphi = \varphi_{\text{pair}} - \Psi_2$ covering the range $0 < \Delta\varphi < \pi/2$. Assuming elliptic flow is the dominant source of the $\Delta\varphi$ variation in the ϕ -meson yields [38–40], the v_2 coefficients are then extracted from a fit to the distribution $dN_\phi/d(\Delta\varphi)$ using the function [18]:

$$\frac{dN_\phi}{d(\Delta\varphi)} = M(1 + 2v_2^{\text{obs}} \cos[2\Delta\varphi]), \quad (4)$$

where M is a normalization constant. Because of the finite bin width in $\Delta\varphi$, the extracted v_2^{obs} values are corrected by a smearing factor $\sigma = \delta/\sin\delta$, which accounts for the finite bin width $\delta = \pi/12$. The v_2 extractions are performed for all of the aforementioned PID approaches and the results with the smallest statistical uncertainties are used in the analysis. The final ϕ -meson v_2 values are evaluated as

$$v_2 = v_2^{\text{obs}}/\text{Res}(\Psi_2).$$

An alternative method to evaluate ϕ -meson v_2 is the invariant mass fit method, described in [18, 34, 38, 40]. In this analysis it is used to perform cross check and for the evaluation of systematic uncertainties.

F. Systematic uncertainties

The calculation of the systematic uncertainties follows the procedure performed in [36–38, 49]. The main sources

of systematic uncertainties for ϕ -meson v_2 and p_T spectra are summarized in Tables IV–VI. Systematic uncertainties are grouped into three types:

- A: (point-to-point uncorrelated), which can move each point independently;
- B: (point-to-point p_T -correlated), which can move points coherently, but not necessarily by the same relative amount;
- C: (global), which move all points by the same relative amount.

The main contribution to the systematic uncertainties of type A is the uncertainty in the raw-yield extraction, evaluated by varying the identification approaches, fit parameters and the parameterization of the residual background. An uncertainty of type B is dominated by uncertainties in acceptance, reconstruction efficiency ε_{rec} , and momentum scale. The main contributions to the type C uncertainties are the uncertainties in normalization for the cross section (9.7%) and $\langle N_{\text{coll}} \rangle$ calculations.

The systematic uncertainties of type A for v_2^{obs} are estimated by varying the elliptic flow measurement method, identification cuts for ϕ mesons, the parameterization of the residual background, and the peak integration window in the m_{KK} distributions. The ϕ -meson v_2 systematic uncertainties of type B and C have two main sources: acceptance and reaction plane determination.

For ϕ -meson p_T spectra and R_{AB} , the systematic uncertainties of type A and B are added in quadrature to give the total systematic uncertainties. For ϕ -meson v_2 , all uncertainties are added in quadrature to give the total systematic uncertainties.

III. RESULTS

A. Invariant transverse-momentum spectra

Figure 3 shows the invariant p_T spectra of ϕ mesons measured in (a) Cu+Au collisions at $\sqrt{s_{NN}} = 200$ GeV and (b) U+U collisions at $\sqrt{s_{NN}} = 193$ GeV at midrapidity $|\eta| < 0.35$. The ϕ -meson spectra are measured from 1.1 to 7.0 GeV/c in p_T for 5 centrality classes in Cu+Au and U+U collisions.

The dashed lines on panels (a) and (b) of Fig. 3 represent the Levy function fits [50]:

$$\frac{1}{2\pi p_T} \frac{d^2 N}{dp_T dy} = \frac{1}{2\pi} \frac{dN}{dy} \frac{(n-1)(n-2)}{nT(nT + m_\phi(n-2))} \times \left(1 + \frac{\sqrt{p_T^2 + m_\phi^2} - m_\phi}{nT} \right)^{-n}, \quad (5)$$

where m_ϕ is the ϕ -meson mass, and dN/dy , T , and n are free parameters. The dN/dy term corresponds to the ϕ -meson multiplicity at midrapidity. The Levy function

TABLE IV. Values of systematic uncertainties (%) for ϕ -meson v_2 measured in Cu+Au collisions at $\sqrt{s_{NN}} = 200$ GeV and U+U collisions at $\sqrt{s_{NN}} = 193$ GeV.

Uncertainty	Cu+Au				U+U
	0%–20%	20%–40%	40%–60%	20%–60%	0%–50%
Reaction plane	7.0	2.0	3.0	1.0	3.0
Acceptance	3.0	3.0	3.0	3.0	3.0
Yield extraction	9.8–12.5	11.4–17.3	12.2–14.1	8.4–14.0	10.9–13.2
Total	12.8–14.9	12.3–17.9	13.3–15.1	9.4–14.7	12.1–14.2

TABLE V. Summary of systematic uncertainties (%) on the ϕ -meson invariant yields in Cu+Au collisions at $\sqrt{s_{NN}} = 200$ GeV.

Uncertainty	p_T (GeV/c)		
	1.45	3.45	7.00
Acceptance	4.5	3.0	3.0
Peak extraction 0%–93%	6.2	8.5	12.6
Peak extraction 0%–20%	7.6	10.7	16.2
Peak extraction 20%–40%	7.9	10.1	14.1
Peak extraction 40%–60%	9.6	11.2	14.0
Peak extraction 60%–80%	8.3	12.5	19.9
Reconstruction efficiency	3.0	3.0	3.0
Momentum scale	0.6	3.0	5.0
Branching ratio	1.2	1.2	1.2
Total 0%–93%	7.9	10.2	14.4
Total 0%–20%	9.0	12.1	17.6
Total 20%–40%	9.3	11.6	15.7
Total 40%–60%	10.8	12.6	15.6
Total 60%–80%	9.6	13.7	21.1

TABLE VI. Summary of systematic uncertainties (%) on the ϕ -meson invariant yields in U+U collisions at $\sqrt{s_{NN}} = 193$ GeV

Uncertainty	p_T (GeV/c)		
	1.10	3.45	7.00
Acceptance	4.0	3.0	3.0
Peak extraction 0%–20%	10.8	7.2	18.5
Peak extraction 20%–40%	11.3	8.1	16.9
Peak extraction 40%–60%	13.6	7.1	15.8
Peak extraction 60%–80%	-	9.7	20.5
Reconstruction efficiency	2.5	2.0	2.0
Momentum scale	0.5	3.6	5.0
Branching ratio	1.2	1.2	1.2
Total 0%–20%	11.8	8.6	19.7
Total 20%–40%	12.2	9.4	18.1
Total 40%–60%	14.4	8.5	16.0
Total 60%–80%	-	10.8	21.0

includes both an exponential shape for low p_T (which can be characterized by an inverse-slope parameter T) and a power-law component (governed by the power parameter n) for the higher p_T region. Panels (c) and (d) of Fig. 3 show data-to-fit ratios, and indicate good agreement between the measured ϕ -meson p_T spectra and the Levy function.

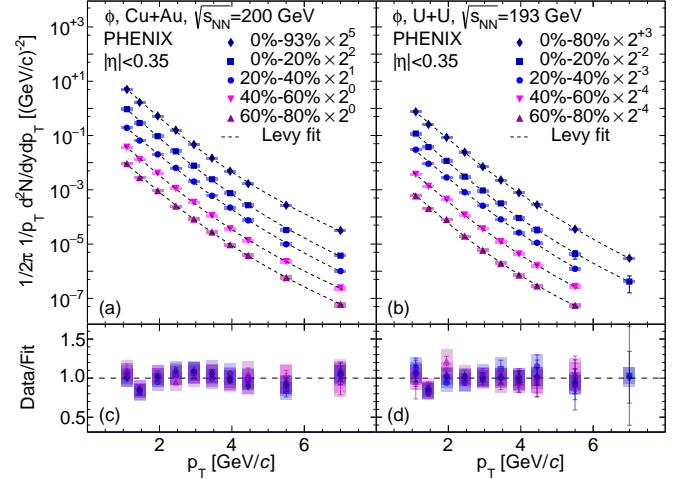


FIG. 3. The invariant transverse momentum spectra measured for ϕ mesons in (a) Cu+Au at $\sqrt{s_{NN}} = 200$ GeV and (b) U+U collisions at $\sqrt{s_{NN}} = 193$ GeV at midrapidity. The statistical uncertainties are represented by vertical lines (hidden by the markers) while the systematic uncertainties represented by rectangles around the points. Panels (c) and (d) show data-to-fit ratios.

B. Nuclear-modification factors

Figure 4 shows ϕ -meson R_{AB} measured in Cu+Au collisions at $\sqrt{s_{NN}} = 200$ GeV and U+U collisions at $\sqrt{s_{NN}} = 193$ GeV at midrapidity $|\eta| < 0.35$. The reference ϕ -meson production cross section in $p+p$ collisions is taken from [48]. The normalization uncertainty from $p+p$ is not shown. The ϕ -meson R_{AB} values in central and semicentral Cu+Au and U+U collisions at high $p_T > 5$ GeV/c are less than unity, indicating suppression. The high- p_T suppression of ϕ -meson yields decrease when moving to more peripheral collisions. The similar behavior of ϕ meson production has been observed in symmetric systems and is interpreted as indicative of in-medium jet quenching [36, 37]. In the most peripheral Cu+Au and U+U collisions in whole p_T range, ϕ -meson R_{AB} factors values are close to unity within uncertainties.

To better understand the features of ϕ -meson production, the integrated nuclear-modification factors $\langle R_{AB} \rangle$ for ϕ mesons as a function of $\langle N_{part} \rangle$ are shown in Fig. 5 for different collision systems (Cu+Au, Au+Au, and Cu+Cu collisions at $\sqrt{s_{NN}} = 200$ GeV, and U+U

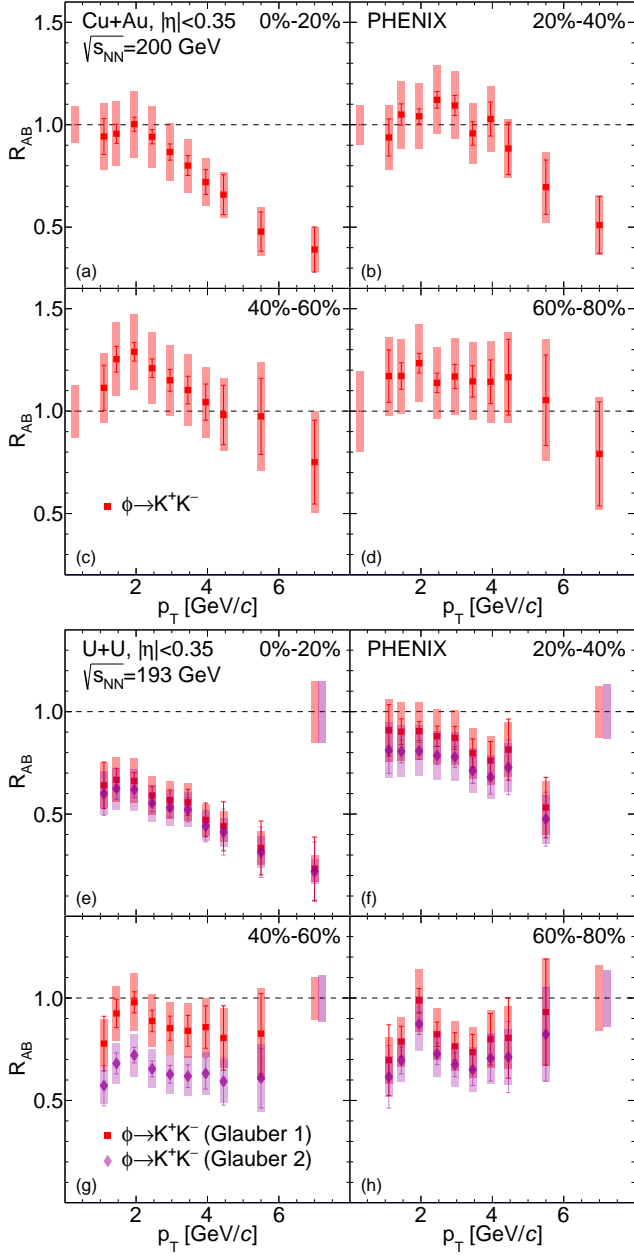


FIG. 4. The ϕ -meson nuclear modification factors R_{AB} measured as a function of p_T in different centrality intervals of (a) to (d) Cu+Au collisions at $\sqrt{s_{NN}} = 200$ GeV and (e) to (h) U+U collisions at $\sqrt{s_{NN}} = 193$ GeV at midrapidity $|\eta| < 0.35$. The normalization uncertainty from $p+p$ of about 9.7% is not shown. Here and below the type C uncertainties are shown as boxes near unity.

collisions at $\sqrt{s_{NN}} = 193$ GeV). The Au+Au and Cu+Cu results are taken from [37]. The integration has been carried out in the intermediate p_T range ($2.2 < p_T(\text{GeV}/c) < 5.0$) and in the high p_T range ($p_T(\text{GeV}/c) > 5.0$). The $\langle R_{AB} \rangle$ values for ϕ mesons vs. $\langle N_{part} \rangle$ obtained in the large collision systems are consistent within uncertainties, as has already been observed for π^0 and η mesons [12, 51]. The value of $\langle N_{part} \rangle$ charac-

terizes the volume of the nuclear-overlap area and hence is assumed to be proportional to the volume of the hot and dense matter formed in heavy ion collisions [19]. For that reason, the obtained $\langle R_{AB} \rangle$ results suggest the scaling of light-hadron production integrated over azimuthal angle with the average nuclear-overlap size, regardless of the collision geometry.

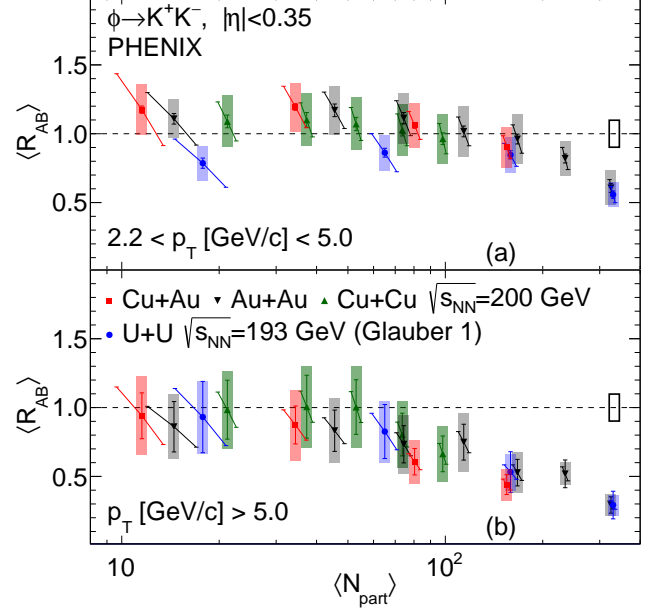


FIG. 5. The ϕ -meson integrated nuclear-modification factors $\langle R_{AB} \rangle$ measured as a function of $\langle N_{part} \rangle$ in Cu+Cu [37], Cu+Au, Au+Au [37] collisions at $\sqrt{s_{NN}} = 200$ GeV, and U+U collisions at $\sqrt{s_{NN}} = 193$ GeV integrated in (a) $2.2 < p_T < 5.0$ GeV/c and (b) $p_T > 5.0$ GeV/c at midrapidity $|\eta| < 0.35$. The tilted bars represent correlated uncertainties from Glauber-Monte-Carlo simulation.

Figure 6 shows the comparisons of ϕ -meson R_{AB} values to π^0 and η meson R_{AB} values [12, 51] obtained in Cu+Au collisions at $\sqrt{s_{NN}} = 200$ GeV and U+U collisions at $\sqrt{s_{NN}} = 193$ GeV at midrapidity. The ϕ -meson R_{AB} values are larger than π^0 and η meson R_{AB} values in the central collisions in the intermediate- p_T range. The differences between π^0 and η meson R_{AB} and ϕ -meson R_{AB} values at moderate p_T decrease as the centrality increases. These trends of light-hadron production in the intermediate p_T range can be qualitatively explained in terms of the interplay of strangeness enhancement and hadronization via coalescence [17]. In central Cu+Au and U+U collisions at high p_T , all light meson yields show the same suppression level. The high p_T suppression is consistent—within the measurement uncertainties—with the assumption of flavor-independent energy loss of pre-fragmentation partons (u, d, s quarks) in the hot and dense medium. The same light-hadron R_{AB} behavior has been observed in symmetric Cu+Cu and Au+Au collisions [37], indicating that features of light-hadron production do not depend on collision geometry.

Figure 7 presents comparisons of ϕ -meson R_{AB} val-

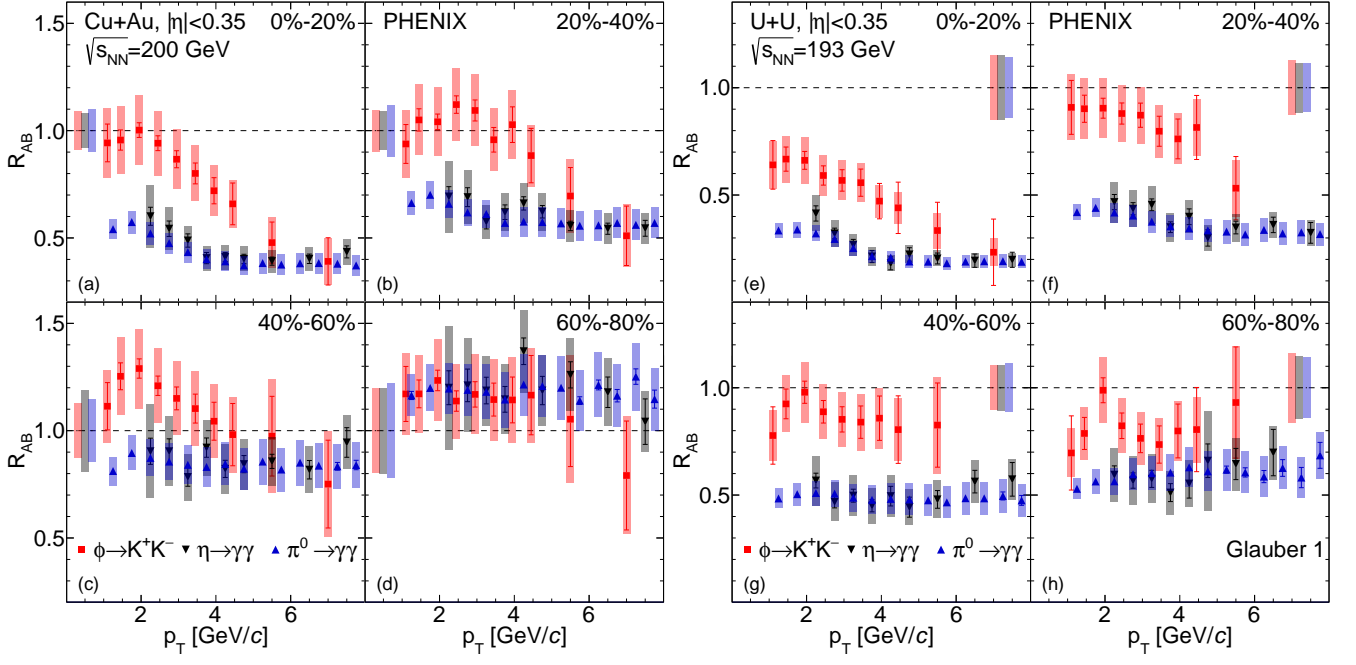


FIG. 6. The comparison of ϕ -meson R_{AB} values to π^0 and η meson R_{AB} values measured as a function of p_T in different centrality intervals of (a) to (d) Cu+Au collisions at $\sqrt{s_{NN}} = 200$ GeV and (e) to (h) U+U collisions at $\sqrt{s_{NN}} = 193$ GeV at midrapidity. The R_{AB} values for π^0 and η meson R_{AB} in Cu+Au and U+U collisions are from [12, 51].

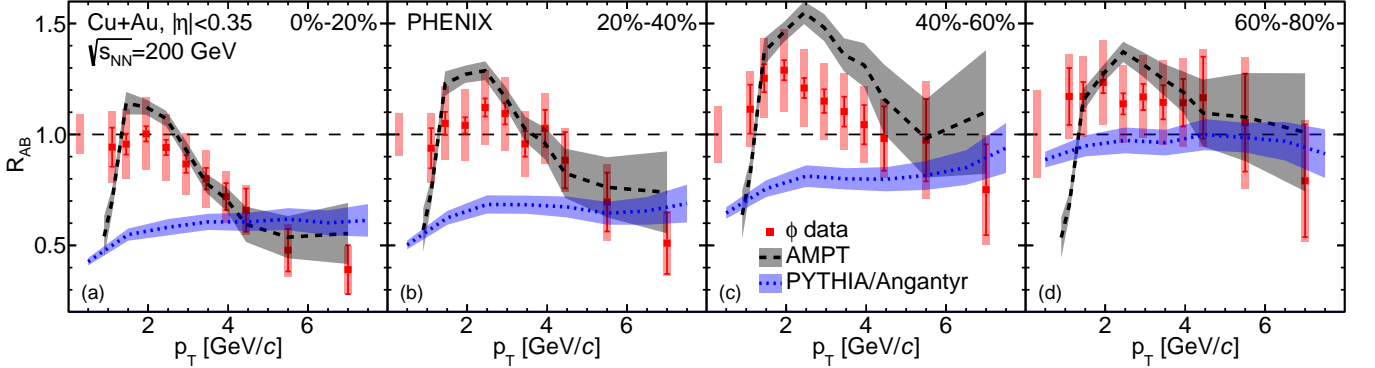


FIG. 7. The comparison of ϕ -meson R_{AB} values measured as a function of p_T in different centrality intervals of Cu+Au collisions at $\sqrt{s_{NN}} = 200$ GeV at midrapidity ($|\eta| < 0.35$) to AMPT model and PYTHIA/Angantyr model predictions.

ues, measured in Cu+Au collisions at $\sqrt{s_{NN}} = 200$ GeV, to R_{AB} values estimated with AMPT [24] and PYTHIA/Angantyr [25] models. The version of the AMPT model employed here includes the string-melting mechanism [54]. String melting refers to excited strings, i.e. those not coming from projectile and target nucleons that do not interact, which are converted (“melted”) into partons. Those produced partons undergo some small number of scatterings and then coalesce (using a simple spatial-coalescence mechanism) into hadrons.

In contrast, the PYTHIA/Angantyr model comprises a coherent set of physics models for the evolution from a few-body hard-scattering process to a complex-multiparticle final state [55]. The ϕ -meson R_{AB} val-

ues in both models are obtained by treating the model outputs in the same way as the experimental data. For R_{AB} calculation with the AMPT model, the ϕ -meson production cross section measured in $p+p$ collisions is used as a baseline. To calculate ϕ -meson R_{AB} with PYTHIA/Angantyr model, the ϕ -meson p_T yields in Cu+Au collision obtained in PYTHIA/Angantyr are divided by ϕ -meson p_T yields in $p+p$ collision from PYTHIA8, and by the same $\langle N_{coll} \rangle$ as in experiment. The AMPT results are obtained using a parton-scattering cross section of 3.0 mb and incorporating the nuclear-shadowing effect [24]. The parameters used in the event generation of PYTHIA/Angantyr are listed in Table VII. The multiplication factor for multipar-

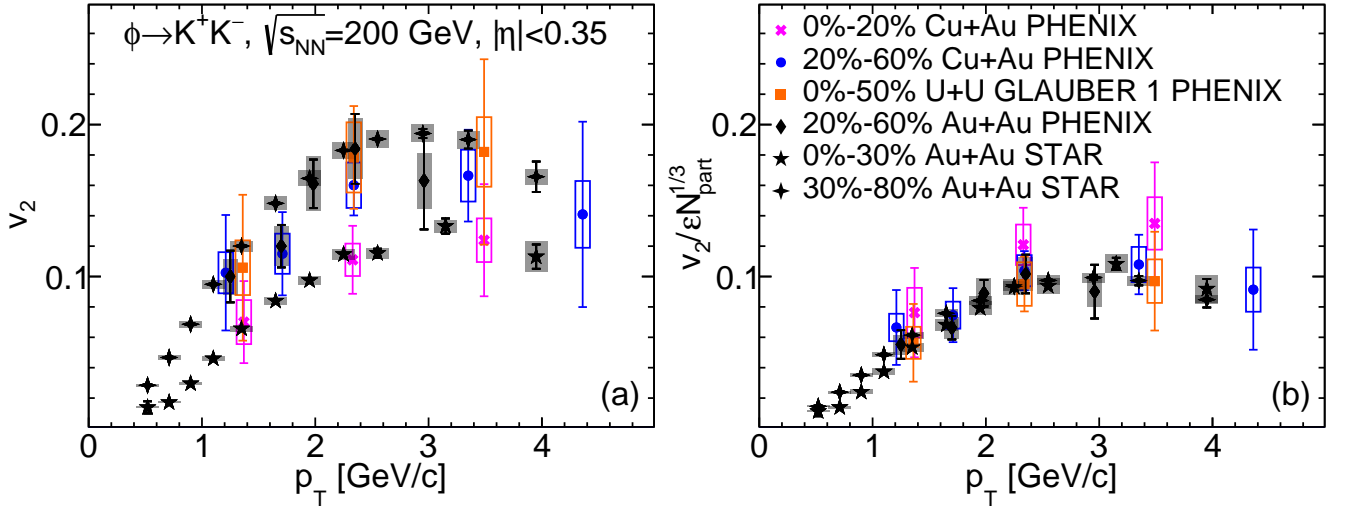


FIG. 8. The comparison of ϕ meson (a) v_2 and (b) $v_2/(\varepsilon_2 N_{\text{part}}^{1/3})$ measured as a function of p_T in Cu+Au, U+U and Au+Au [38, 52] collisions at $\sqrt{s_{NN}} = 200$ GeV at midrapidity ($|\eta| < 0.35$).

ton interactions is introduced to match charged hadron multiplicities in $p+p$ collisions at $\sqrt{s_{NN}} = 200$ GeV in PYTHIA calculations and experimental data [56]. PYTHIA/Angantyr calculations include uncertainties estimated from the variation of parton-distribution functions.

To quantify the agreement of model calculations with experimental results, p -values [57] are calculated from the least-squares minimization in the standard way. Table VIII shows the p -values estimated for the string melting version of AMPT and PYTHIA/Angantyr model calculations of ϕ -meson R_{AB} values in different centrality classes of Cu+Au collisions at $\sqrt{s_{NN}} = 200$ GeV at midrapidity.

The values of ϕ -meson R_{AB} measured in peripheral Cu+Au collisions are well described by both PYTHIA/Angantyr and AMPT model calculations. In the most-central and semicentral Cu+Au collisions at moderate p_T , ϕ -meson R_{AB} values obtained with PYTHIA/Angantyr are significantly smaller than the measured R_{AB} values, whereas the AMPT model reproduces the measured ϕ -meson R_{AB} values as reasonably well supported by the calculated p -values (Table VIII). This means ϕ -meson production measured in Cu+Au collisions is well described by the AMPT model, which assumes that the mechanism of ϕ -meson production at moderate p_T is dominated by the coalescence of $s\bar{s}$ pairs [24].

C. Elliptic flow

Figure 8 presents ϕ -meson v_2 values as a function of p_T measured in 0%–20% and 20%–60% Cu+Au collisions and 0%–50% U+U collisions. Elliptic flow values for ϕ mesons previously obtained in 20%–60% Au+Au

collisions by PHENIX [38] and in 0%–30% and 30%–80% Au+Au collisions by STAR [52] are also shown in Fig. 8. The comparison of elliptic flow for ϕ mesons in symmetric and asymmetric collision systems suggests that the v_2 values follow common empirical scaling with $\varepsilon_2 N_{\text{part}}^{1/3}$. Scaling with participant eccentricity of second order ε_2 represents dependence of v_2 on the shape of the nuclear overlap region. The $N_{\text{part}}^{1/3}$ factor is introduced to characterize the length scale of nuclear overlap region and assumed to be proportional to the QGP length scale [19]. This suggests that the influence of the initial conditions on v_2 coefficients, and thereby on QGP properties, are reasonably well encapsulated in the scaling factor $\varepsilon_2 N_{\text{part}}^{1/3}$. The scaling of v_2 values with the shape and size of nuclear-overlap region can be explained by the hydrodynamic nature of the QGP at low values of specific-shear viscosity [21].

The comparisons of elliptic-flow v_2 and v_2/n_q values obtained for ϕ mesons in 0%–20% and 20%–60% Cu+Au collisions and 0%–50% U+U collisions to corresponding v_2 and v_2/n_q values for π^\pm mesons and (anti)protons ($(p + \bar{p})/2$) [49, 53] are shown in Figs. 9 through 11, respectively. The scaling of light hadron v_2 with the number of valence quarks in the hadron n_q and transverse kinetic energy per valence quark KE_T/n_q is observed. The n_q scaling can be explained via quark-coalescence models in which partons develop flow during the evolution of partonic matter and the hadron flow is the sum of collective flows of constituent partons [58, 59]. A smaller rescattering cross section [60] for ϕ mesons than for π^\pm mesons and (anti)protons may also indicate that the elliptic flow develops prior to hadronization.

The elliptic-flow values measured for ϕ mesons are compared to the calculations of iEBE-VISHNU (2+1)D viscous-hydrodynamic model with specific viscosity $\eta/s = 1/(4\pi)$ and string-melting version of the

TABLE VII. Parameters used in PYTHIA/Angantyr

Parameter	Value	Description
SoftQCD: all	on	All soft QCD processes
PDF: pSet	8	CTEQ6l1 parton distribution function
Multiparton Interactions: Kfactor	0.5	Multiplication factor for multiparton interaction

TABLE VIII. p -values estimated for the string melting version of AMPT and PYTHIA/Angantyr calculations of ϕ -meson R_{AB} in different centrality classes of Cu+Au collisions at $\sqrt{s_{NN}} = 200$ GeV at midrapidity.

Centrality	p value	
	AMPT sm	PYTHIA/Angantyr
0%–20%	0.823	3.22×10^{-4}
20%–40%	0.712	5.79×10^{-5}
40%–60%	0.103	4.88×10^{-3}
60%–80%	0.671	0.455

TABLE IX. p -values estimated for the iEBE-VISHNU and string melting version of AMPT calculations of ϕ -meson v_2 in different centrality classes of Cu+Au at $\sqrt{s_{NN}} = 200$ GeV and U+U collisions at $\sqrt{s_{NN}} = 193$ GeV.

Collision	Centrality	p value	
		iEBE-VISHNU	AMPT sm
Cu+Au	0%–20%	0.788	0.287
	20%–40%	0.985	0.927
	40%–60%	0.998	0.878
	20%–60%	0.905	0.513
U+U	0%–50%	0.756	0.097

AMPT model. The comparisons of measured ϕ -meson v_2 values to AMPT and iEBE-VISHNU model predictions are shown in Fig. 12 for 0%–20%, 20%–40%, 40%–60%, and 20%–60% Cu+Au collisions and for 0%–50% U+U collisions. Table IX shows the p -values estimated for iEBE-VISHNU and AMPT model calculations of ϕ -meson v_2 values in different centrality classes of Cu+Au and U+U collisions.

Elliptic flow for ϕ mesons estimated with the AMPT model are consistent within uncertainties with the ϕ -meson v_2 values measured in Cu+Au collisions. The ϕ -meson v_2 values in U+U collisions are under-predicted by AMPT calculations, as shown in Fig. 12(e). In contrast, calculations of iEBE-VISHNU (2+1)D viscous-hydrodynamic model with specific-shear viscosity $\eta/s = 1/(4\pi)$ reproduce ϕ -meson elliptic flow measured in both Cu+Au and U+U collisions with high precision.

IV. SUMMARY

The PHENIX experiment has measured invariant transverse-momentum spectra, nuclear-modification factors, and elliptic flow for ϕ mesons in asymmetric Cu+Au

collisions at $\sqrt{s_{NN}} = 200$ GeV and in the largest collision system at RHIC, U+U at $\sqrt{s_{NN}} = 193$ GeV at midrapidity $|\eta| < 0.35$ via the kaon-decay channel. The comparisons of measured ϕ -meson R_{AB} and v_2 values to previously obtained PHENIX results and to model predictions have been provided.

It is found that features of ϕ -meson production measured in heavy ion collisions reported by the PHENIX experiment do not depend on the shape of the nuclear-overlap region. The obtained ϕ -meson $\langle R_{AB} \rangle$ and $v_2/(\varepsilon_2 N_{\text{part}}^{1/3})$ values are consistent across Cu+Cu, Cu+Au, Au+Au, and U+U collisions within uncertainties. The measured ϕ -meson production averaged over the azimuthal angle scales with the nuclear-overlap size. Elliptic flow for ϕ mesons scales with the second-order-participant eccentricity and the characteristic length of the nuclear-overlap area.

The ϕ -meson R_{AB} values measured in Cu+Au and U+U collisions at moderate p_T are larger than R_{AB} values of π^0 and η mesons. In both Cu+Au and U+U collisions, the ϕ -meson v_2 values follow the patterns of π^0 -meson and $(p + \bar{p})/2$ v_2 values when scaled with the number of valence quarks in the hadron n_q . Both of these observations at moderate p_T can be qualitatively explained by recombination of $s\bar{s}$ pairs in ϕ -meson production. The obtained ϕ -meson R_{AB} and v_2 values are quantitatively described by the AMPT and iEBE-VISHNU models, which include the coalescence mechanism.

At high p_T , yields of ϕ , π^0 , and η mesons are equally suppressed in Cu+Au and U+U collisions. This pattern is in agreement with expectations for in-medium energy loss of parent partons prior to their fragmentation. The high- p_T suppression scales with size of the nuclear-overlap region, which is assumed to be proportional to the QGP volume.

The scaling of hadronic elliptic flow with the number of valence quarks in the hadron n_q , the second-order-participant eccentricity ε_2 , and the cube root of participant-nucleons number $N_{\text{part}}^{1/3}$ can be explained by the hydrodynamic nature of the QGP. The measured v_2 values for ϕ mesons are well described by (2+1)D viscous hydrodynamic model with specific shear viscosity $\eta/s = 1/(4\pi)$.

ACKNOWLEDGMENTS

We thank the staff of the Collider-Accelerator and Physics Departments at Brookhaven National Labora-

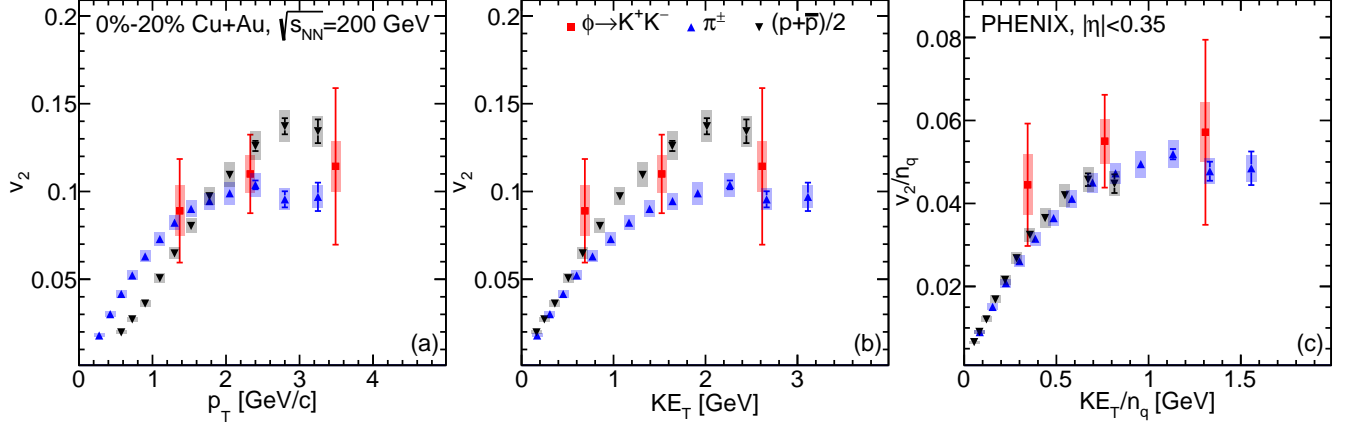


FIG. 9. The comparison of elliptic flow (a, b) v_2 and (c) v_2/n_q values measured for ϕ mesons as a function of (a) p_T , (b) KE_T and (c) KE_T/n_q in 0%–20% Cu+Au collisions to corresponding v_2 and v_2/n_q values for π^\pm mesons and (anti)protons $((p+\bar{p})/2)$. The values for π^\pm mesons and $(p+\bar{p})/2$ v_2 are taken from [49].

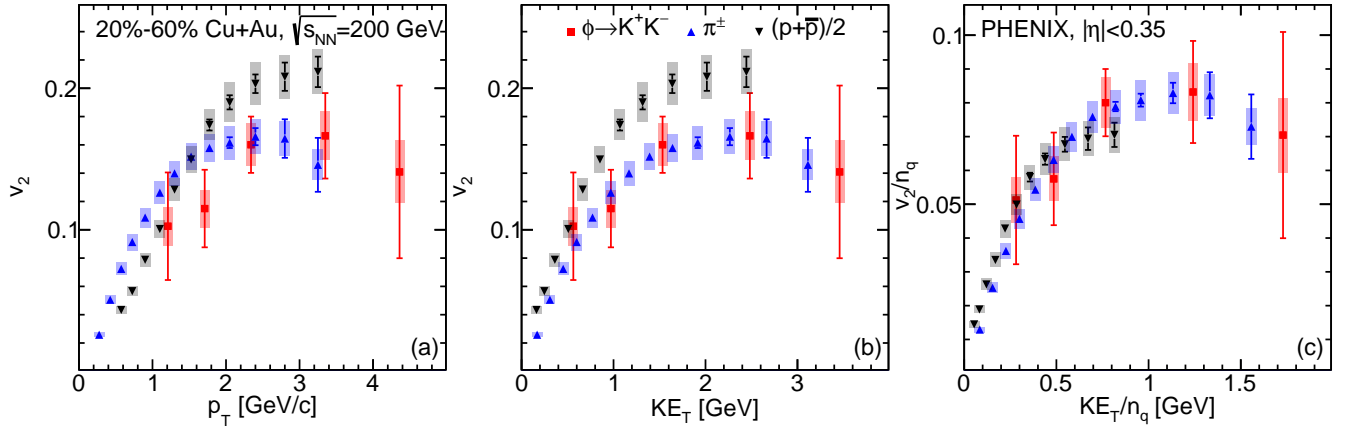


FIG. 10. The comparison of elliptic flow (a, b) v_2 and (c) v_2/n_q for ϕ mesons measured as a function of (a) p_T , (b) KE_T and (c) KE_T/n_q in 20%–60% Cu+Au collisions to corresponding v_2 and v_2/n_q values for π^\pm mesons and (anti)protons $((p+\bar{p})/2)$. The values for π^\pm mesons and $(p+\bar{p})/2$ v_2 are taken from [49].

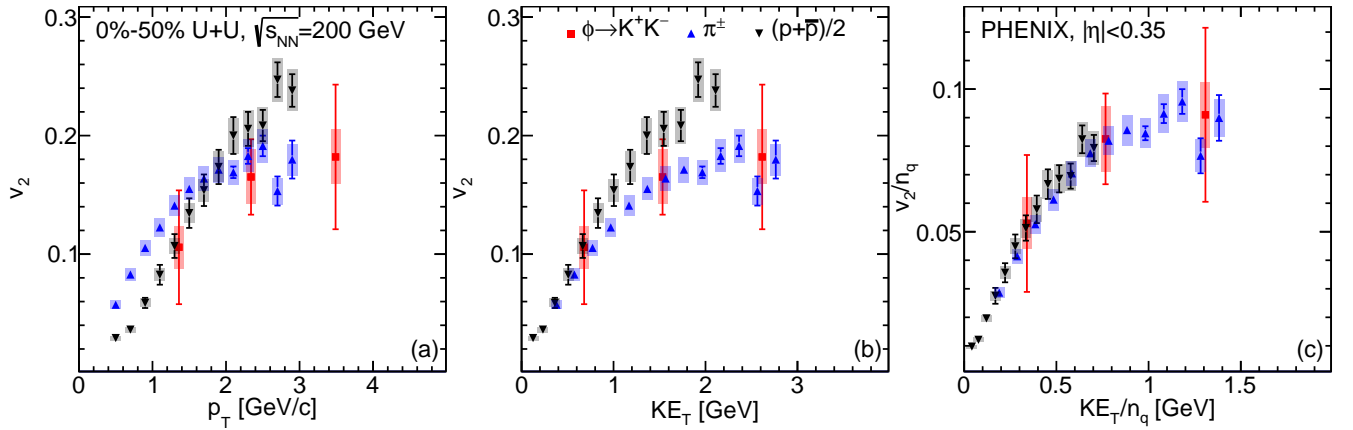


FIG. 11. The comparison of elliptic flow (a, b) v_2 and (c) v_2/n_q for ϕ mesons measured as a function of (a) p_T , (b) KE_T and (c) KE_T/n_q in 0%–50% U+U collisions to corresponding v_2 and v_2/n_q values for π^\pm mesons and (anti)protons $((p+\bar{p})/2)$. The values for π^\pm mesons and $(p+\bar{p})/2$ v_2 are taken from [53].

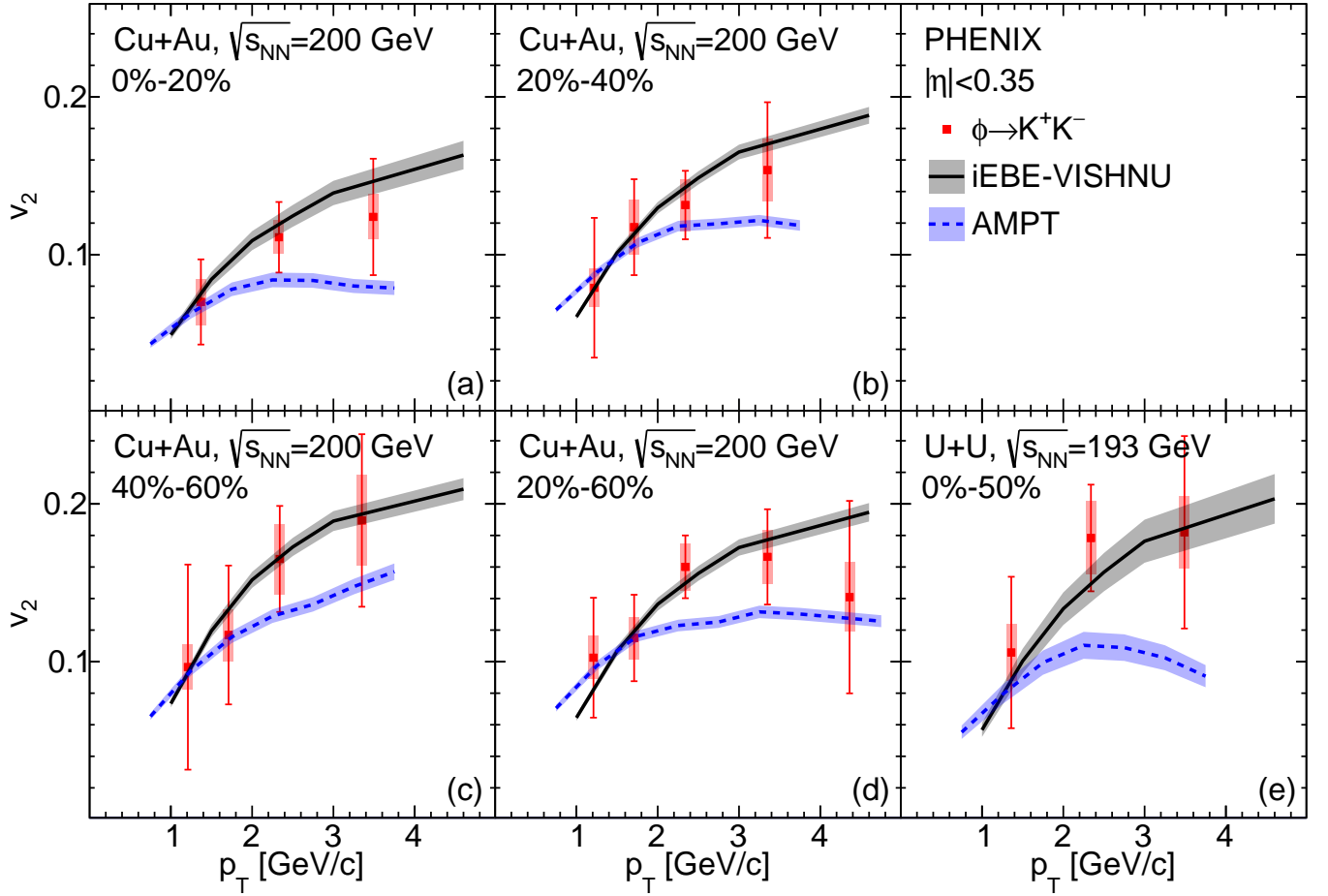


FIG. 12. The comparison of elliptic flow $v_2(p_T)$ for ϕ mesons measured in (a) 0%–20%, (b) 20%–40%, (c) 40%–60%, and (d) 20%–60% Cu+Au collisions and (e) 0%–50% U+U collisions to iEBE-VISHNU hydrodynamic model predictions with specific viscosity $\eta/s = 1/(4\pi)$ and AMPT model predictions.

tory and the staff of the other PHENIX participating institutions for their vital contributions. We acknowledge support from the Office of Nuclear Physics in the Office of Science of the Department of Energy, the National Science Foundation, Abilene Christian University Research Council, Research Foundation of SUNY, and Dean of the College of Arts and Sciences, Vanderbilt University (U.S.A), Ministry of Education, Culture, Sports, Science, and Technology and the Japan Society for the Promotion of Science (Japan), Natural Science Foundation of China (People's Republic of China), Croatian Science Foundation and Ministry of Science and Education (Croatia), Ministry of Education, Youth and Sports (Czech Republic), Centre National de la Recherche Scientifique, Commissariat à l'Énergie Atomique, and Institut National de Physique Nucléaire et de Physique des Particules (France), J. Bolyai Research Scholarship, EFOP,

the New National Excellence Program (ÚNKP), NKFIH, and OTKA (Hungary), Department of Atomic Energy and Department of Science and Technology (India), Israel Science Foundation (Israel), Basic Science Research and SRC(CENuM) Programs through NRF funded by the Ministry of Education and the Ministry of Science and ICT (Korea). Ministry of Education and Science, Russian Academy of Sciences, Federal Agency of Atomic Energy (Russia), VR and Wallenberg Foundation (Sweden), University of Zambia, the Government of the Republic of Zambia (Zambia), the U.S. Civilian Research and Development Foundation for the Independent States of the Former Soviet Union, the Hungarian American Enterprise Scholarship Fund, the US-Hungarian Fulbright Foundation, and the US-Israel Binational Science Foundation.

[1] M. Harrison, T. Ludlam, and S. Ozaki, RHIC project overview, Nucl. Instrum. Methods Phys. Res., Sec. A

- [2] K. Adcox *et al.* (PHENIX Collaboration), Formation of dense partonic matter in relativistic nucleus-nucleus collisions at RHIC: Experimental evaluation by the PHENIX collaboration, *Nucl. Phys. A* **757**, 184 (2005).
- [3] I. Arsene *et al.* (BRAHMS Collaboration), Quark gluon plasma and color glass condensate at RHIC? The Perspective from the BRAHMS experiment, *Nucl. Phys. A* **757**, 1 (2005).
- [4] B. B. Back *et al.* (PHOBOS Collaboration), The PHOBOS perspective on discoveries at RHIC, *Nucl. Phys. A* **757**, 28 (2005).
- [5] J. Adams *et al.* (STAR Collaboration), Experimental and theoretical challenges in the search for the quark gluon plasma: The STAR Collaboration's critical assessment of the evidence from RHIC collisions, *Nucl. Phys. A* **757**, 102 (2005).
- [6] S. Chatrchyan *et al.* (CMS Collaboration), Study of high- p_T charged particle suppression in PbPb compared to pp collisions at $\sqrt{s_{NN}} = 2.76$ TeV, *Eur. Phys. J. C* **72**, 1945 (2012).
- [7] B. Abelev *et al.* (ALICE Collaboration), Centrality Dependence of Charged Particle Production at Large Transverse Momentum in Pb-Pb Collisions at $\sqrt{s_{NN}} = 2.76$ TeV, *Phys. Lett. B* **720**, 52 (2013).
- [8] G. Aad *et al.* (ATLAS Collaboration), Measurement of the jet radius and transverse momentum dependence of inclusive jet suppression in lead-lead collisions at $\sqrt{s_{NN}} = 2.76$ TeV with the ATLAS detector, *Phys. Lett. B* **719**, 220 (2013).
- [9] T. Gunji (ALICE Collaboration), Overview of recent ALICE results, *Nucl. Phys. A* **956**, 11 (2016).
- [10] K. Adcox *et al.* (PHENIX Collaboration), PHENIX detector overview, *Nucl. Instrum. Methods Phys. Res., Sec. A* **499**, 469 (2003).
- [11] J. J. Ethier and E. R. Nocera, Parton distributions in nucleons and nuclei, *Ann. Rev. Nucl. Part. Sci.* **70**, 43 (2020).
- [12] C. Aidala *et al.* (PHENIX Collaboration), Production of π^0 and η mesons in Cu + Au collisions at $\sqrt{s_{NN}} = 200$ gev, *Phys. Rev. C* **98**, 054903 (2018).
- [13] D. d'Enterria, Jet quenching, *Landolt-Bornstein* **23**, 471 (2010).
- [14] P. Koch, B. Muller, and J. Rafelski, Strangeness in Relativistic Heavy Ion Collisions, *Phys. Rept.* **142**, 167 (1986).
- [15] V. Greco, C. M. Ko, and P. Lévai, Parton coalescence and the antiproton/pion anomaly at rhic, *Phys. Rev. Lett.* **90**, 202302 (2003).
- [16] R. C. Hwa and C. B. Yang, Scaling behavior at high p_t and the p/π ratio, *Phys. Rev. C* **67**, 034902 (2003).
- [17] R. C. Hwa and C. B. Yang, Production of strange particles at intermediate p_T in central Au+Au collisions at high energies, *Phys. Rev. C* **75**, 054904 (2007).
- [18] N. Borghini, Characterization and analysis of azimuthally sensitive correlations, *J. Phys. G* **31**, S15 (2005).
- [19] A. Adare *et al.* (PHENIX Collaboration), Systematic Study of Azimuthal Anisotropy in Cu+Cu and Au+Au Collisions at $\sqrt{s_{NN}} = 62.4$ and 200 GeV, *Phys. Rev. C* **92**, 034913 (2015).
- [20] S. S. Adler *et al.* (PHENIX Collaboration), Saturation of Azimuthal Anisotropy in Au+Au Collisions at $\sqrt{s_{NN}} = 62$ -200 GeV, *Phys. Rev. Lett.* **94**, 232302 (2005).
- [21] U. Heinz and R. Snellings, Collective flow and viscosity in relativistic heavy-ion collisions, *Ann. Rev. Nucl. Part. Sci.* **63**, 123 (2013).
- [22] A. Shor, ϕ -meson production as a probe of the Quark-Gluon Plasma, *Phys. Rev. Lett.* **54**, 1122 (1985).
- [23] C. Shen, Z. Qiu, H. Song, J. Bernhard, S. Bass, and U. Heinz, The iEBE-VISHNU code package for relativistic heavy-ion collisions, *Comput. Phys. Commun.* **199**, 61 (2016).
- [24] Z.-W. Lin, C. M. Ko, B.-A. Li, B. Zhang, and S. Pal, A Multi-phase transport model for relativistic heavy ion collisions, *Phys. Rev. C* **72**, 064901 (2005).
- [25] A. V. da Silva, W. M. Serenone, D. D. Chinellato, J. Takahashi, and C. Bierlich, Studies of heavy-ion collisions using PYTHIA Angantyr and UrQMD (2020).
- [26] M. Allen *et al.* (PHENIX Collaboration), PHENIX inner detectors, *Nucl. Instrum. Methods Phys. Res., Sec. A* **499**, 549 (2003).
- [27] A. Adare *et al.* (PHENIX Collaboration), Centrality categorization for $R_{p(d)+A}$ in high-energy collisions, *Phys. Rev. C* **90**, 034902 (2014).
- [28] M. L. Miller, K. Reygers, S. J. Sanders, and P. Steinberg, Glauber modeling in high-energy nuclear collisions, *Ann. Rev. Nucl. Part. Sci.* **57**, 205 (2007).
- [29] H. Masui, B. Mohanty, and N. Xu, Predictions of elliptic flow and nuclear modification factor from 200 GeV U+U collisions at RHIC, *Phys. Lett. B* **679**, 440 (2009).
- [30] Q. Y. Shou, Y. G. Ma, P. Sorensen, A. H. Tang, F. Videbaek, and H. Wang, Parameterization of deformed nuclei for Glauber modeling in relativistic heavy ion collisions, *Phys. Lett. B* **749**, 215 (2015).
- [31] C. Aidala *et al.*, The PHENIX forward silicon vertex detector, *Nucl. Instrum. Methods Phys. Res., Sec. A* **755**, 44 (2014).
- [32] M. Chiu (PHENIX Collaboration), Single spin transverse asymmetries of neutral pions at forward rapidities in $\sqrt{s} = 200 = 62.4$ GeV polarized proton collisions in PHENIX Collaboration, *AIP Conf. Proc.* **915**, 539 (2007).
- [33] A. M. Poskanzer and S. A. Voloshin, Methods for analyzing anisotropic flow in relativistic nuclear collisions, *Phys. Rev. C* **58**, 1671 (1998).
- [34] A. M. Poskanzer and S. A. Voloshin, Methods for analyzing anisotropic flow in relativistic nuclear collisions, *Phys. Rev. C* **58**, 1671 (1998).
- [35] P. A. Zyla *et al.* (Particle Data Group), *Rev. of Particle Phys.*, *Prog. Theor. Exp. Phys.* **2020**, 083C01 (2020).
- [36] S. S. Adler *et al.* (PHENIX Collaboration), Production of phi mesons at midrapidity in $\sqrt{s_{NN}} = 200$ GeV Au+Au collisions at RHIC, *Phys. Rev. C* **72**, 014903 (2005).
- [37] A. Adare *et al.* (PHENIX Collaboration), Nuclear modification factors of ϕ mesons in d +Au, Cu+Cu and Au+Au collisions at $\sqrt{s_{NN}} = 200$ GeV, *Phys. Rev. C* **83**, 024909 (2011).
- [38] S. Afanasiev *et al.* (PHENIX Collaboration), Elliptic flow for ϕ mesons and (anti)deuterons in Au + Au collisions at $\sqrt{s_{NN}} = 200$ GeV, *Phys. Rev. Lett.* **99**, 052301 (2007).
- [39] S. Afanasiev *et al.* (PHENIX), High- p_T π^0 Production with Respect to the Reaction Plane in Au+Au Collisions at $\sqrt{s_{NN}} = 200$ GeV, *Phys. Rev. C* **80**, 054907 (2009).
- [40] A. Adare *et al.* (PHENIX Collaboration), Azimuthal anisotropy of π^0 and η mesons in Au+Au collisions at $\sqrt{s_{NN}} = 200$ GeV, *Phys. Rev. C* **88**, 064910 (2013).
- [41] K. Adcox *et al.*, PHENIX central arm tracking detec-

- tors, Nucl. Instrum. Methods Phys. Res., Sec. A **499**, 489 (2003).
- [42] L. Carlén *et al.*, A large-acceptance spectrometer for tracking in a high multiplicity environment, based on space point measurements and high resolution time-of-flight, Nucl. Instrum. Methods Phys. Res., Sec. A **431**, 123 (1999).
 - [43] M. Aizawa *et al.* (PHENIX Collaboration), PHENIX central arm particle ID detectors, Nucl. Instrum. Methods Phys. Res., Sec. A **499**, 508 (2003).
 - [44] S. S. Adler *et al.* (PHENIX Collaboration), Production of phi mesons at midrapidity in $\sqrt{s_{NN}} = 200$ GeV Au+Au collisions at RHIC, Phys. Rev. C **72**, 014903 (2005).
 - [45] S. S. Adler *et al.*, Production of φ -mesons at midrapidity in $\sqrt{s_{NN}}=200$ GeV Au+Au collisions at relativistic energies, Phys. Rev. C **72**, 014903 (2005).
 - [46] R. Brun, F. Bruyant, M. Maire, A. C. McPherson, and P. Zancarini, GEANT3 (1987).
 - [47] M. M. Mitrnkova, Y. A. Berdnikov, A. Y. Berdnikov, D. O. Kotov, and I. M. Mitrnkov, Production of light flavor hadrons in small systems measured by PHENIX at RHIC, Phys. Scripta **96**, 084010 (2021).
 - [48] A. Adare *et al.* (PHENIX Collaboration), Measurement of neutral mesons in $p+p$ collisions at $\sqrt{s} = 200$ GeV and scaling properties of hadron production, Phys. Rev. D **83**, 052004 (2011).
 - [49] A. Adare *et al.* (PHENIX Collaboration), Measurements of directed, elliptic, and triangular flow in Cu + Au collisions at $\sqrt{s_{NN}} = 200$ GeV, Phys. Rev. C **94**, 054910 (2016).
 - [50] B. Abelev *et al.* (STAR Collaboration), Strange particle production in $p+p$ collisions at $\sqrt{s} = 200$ GeV, Phys. Rev. C **75**, 064901 (2007).
 - [51] U. Acharya *et al.* (PHENIX Collaboration), Production of π^0 and η mesons in U+U collisions at $\sqrt{s_{NN}} = 192$ GeV, Phys. Rev. C **102**, 064905 (2020).
 - [52] L. Adamczyk *et al.* (STAR Collaboration), Centrality and transverse momentum dependence of elliptic flow of multistrange hadrons and ϕ meson in Au + Au collisions at $\sqrt{s_{NN}} = 200$ GeV, Phys. Rev. Lett. **116**, 062301 (2016).
 - [53] S. Huang, Measurements of identified particle anisotropic flow in Cu + Au and U + U collisions by PHENIX experiment, Nucl. Phys. A **904-905**, 417c (2013), the Quark Matter 2012.
 - [54] Z.-W. Lin and C. M. Ko, Partonic effects on the elliptic flow at relativistic heavy ion collisions, Phys. Rev. C **65**, 034904 (2002).
 - [55] T. Sjöstrand, S. Ask, J. R. Christiansen, R. Corke, N. Desai, P. Ilten, S. Mrenna, S. Prestel, C. O. Rasmussen, and P. Z. Skands, An introduction to PYTHIA 8.2, Comp. Phys. Commun. **191**, 159 (2015).
 - [56] B. Alver *et al.*, Charged-particle multiplicity and pseudorapidity distributions measured with the PHOBOS detector in Au+Au, Cu+Cu, d+Au, and $p+p$ collisions at ultrarelativistic energies, Phys. Rev. C **83**, 024913 (2011).
 - [57] L. Demortier, P values and nuisance parameters, in *PHYSTAT-LHC Workshop on Statistical Issues for LHC Phys.* (2008) p. 23, <http://cds.cern.ch/record/1099967>.
 - [58] K. Dusling and R. Venugopalan, Azimuthal collimation of long range rapidity correlations by strong color fields in high multiplicity hadron-hadron collisions, Phys. Rev. Lett. **108**, 262001 (2012).
 - [59] A. Ortiz Velasquez, P. Christiansen, E. Cuautle Flores, I. A. Maldonado Cervantes, and G. Pais, Color reconnection and flow like patterns in $p+p$ collisions, Phys. Rev. Lett. **111**, 042001 (2013).
 - [60] A. Sibirtsev, H.-W. Hammer, U.-G. Meissner, and A. Thomas, phi-meson photoproduction from nuclei, Eur. Phys. J. A **29**, 209 (2006).